75th International Astronautical Congress (IAC), Milan, Italy, 14-18 October 2024.


IAC-24-A6,11,10,x89565

# Efficient high-dimensional multi-objective optimisation method for large-scale sensor tasking

**Yifan Cai[a]*, Juan Luis Gonzalo[b], Camilla Colombo[c]**

[a] *Department of Aerospace Engineering, Politecnico di Milano, Via Privata Giuseppe La Masa 34, Milan, Italy,* yifan.cai@polimi.it
[b] *Department of Aerospace Engineering, Politecnico di Milano, Via Privata Giuseppe La Masa 34, Milan, Italy,* juanluis.gonzalo@polimi.it
[c] *Department of Aerospace Engineering, Politecnico di Milano, Via Privata Giuseppe La Masa 34, Milan, Italy,* camilla.colombo@polimi.it
* Corresponding Author

**Abstract**

With the deployment of Low Earth Orbit (LEO) mega constellations, the space environment is becoming increasingly congested, making Space Situational Awareness (SSA) essential for ensuring space safety. SSA relies on Space Surveillance and Tracking (SST) systems, which use a limited number of sensors to detect and track Resident Space Objects (RSOs). However, the growing number of RSOs has placed significant pressure on these systems. Optimally tasking multiple sensors to observe RSOs at each epoch is critical for maintaining SSA but presents challenges due to the large-scale and multi-objective nature of the problem. This paper presents an efficient optimisation method based on coordinate descent and Pareto optimality to address the high-dimensional multi-objective sensor tasking problem. By decomposing the optimisation problem in the three-dimensional solution space into a set of optimisation subproblems defined on a two-dimensional solution plane and iteratively optimizing all subproblems along two-dimensional coordinates, the optimisation problem in the three-dimensional solution space can gradually approach the optimal solution. Multiple objectives are balanced within each subproblem, resulting in improved RSO catalogue maintenance. The proposed method is validated in multi-sensor, multi-target, and multi-epoch sensor tasking scenarios, and its performance is compared to the classical greedy approach using metrics such as detection probability, position and velocity errors, and cataloguing success rate. This approach enhances large-scale sensor tasking and strengthens SSA capabilities under resource constraints. Notably, the method effectively addresses this complex, high-dimensional multi-objective optimisation problem.

**Keywords:** Space Situational Awareness, LEO Mega Constellations, Sensor Tasking, Coordinate Descent, Pareto Optimality

## 1. Introduction

Space Situational Awareness (SSA) is a fundamental capability to ensure the safety of on-orbit spacecraft and the sustainability of the space industry. A key component of SSA is the ability to establish and maintain a catalogue of Resident Space Objects (RSOs) through space surveillance and tracking (SST) systems. To achieve this, communities have long relied on ground-based or space-based sensors forming SST systems for the detection and tracking of targets in orbit. However, with the rapid growth of space activities, such as the large-scale deployment of mega constellations in Low Earth Orbit (LEO) consisting of tens of thousands of satellites, the number of in-orbit spacecraft requiring timely and accurate detection has sharply increased. Additionally, both NASA and ESA estimate that approximately 100 million debris objects between 1 mm and 10 cm in size are currently untracked and unrecorded in any catalogue.

What makes the situation even more critical is that the SST sensor resources available for SSA are limited. On one hand, the number of sensors cannot be increased indefinitely due to cost constraints. On the other hand, each sensor's detection capacity is restricted by hardware limitations. Simultaneously, due to the nonlinearity of orbital dynamics, the position uncertainty of RSOs increases over time, necessitating frequent re-observation of all known objects. This creates immense pressure on SSA. Therefore, one of the primary challenges in SSA is tracking a vast number of RSOs using a limited number of sensors.

To maximise the use of limited sensor resources for collecting observation data on numerous RSOs, and thus maintaining robust SSA capabilities, efficient sensor tasking schemes are essential. The aim of this large-scale tasking scheme is to allocate the observation tasks of each sensor to the RSOs at each epoch in an optimal manner, thereby generating more effective measurements and improving orbital state estimates on a global scale [1-3]. However, optimal sensor tasking is a complex endeavour due to several factors. First, this large-scale optimisation problem involves multiple sensors, multiple epochs, and a considerable number of RSOs to be observed, resulting in exponential growth in

the three-dimensional solution space as any of these elements increase, leading to high computational complexity and difficult optimisation. Second, many operations, such as collision avoidance and emergency rescues, require timely and accurate updates of RSO orbital states, and these demands as optimisation objectives are often conflicting. This makes the multi-sensor, multi-target tracking problem a challenging multi-objective optimisation task.

To address this complex high-dimensional multi-objective optimisation problem, various methods have been explored, including heuristic planning combinations [4] and rigorous information-theoretic approaches. The former can generate sensor tasking schemes without the need for target state information, but they may fall short in terms of estimation accuracy and catalogue maintenance, and require extensive parameter tuning. The latter, although mathematically rigorous, often rely solely on Information Gain (IG) functions, allocating sensor tasks based on mathematical principles without explicitly considering multiple real-world mission objectives.

For the handling of multiple epochs within a time window, two frameworks are available: single-step and multi-step. The single-step framework selects targets to observe using predicted information from the next epoch, simplifying the solution space of the optimisation problem but often leading to short-sighted results. In contrast, the multi-step framework allocates sensors across multiple epochs in the time window, which significantly increases computational cost but typically produces more effective global outcomes [1].

This paper proposes an efficient optimisation method based on the coordinate descent approach and the concept of Pareto optimality. Building on the multi-step optimisation framework, by decomposing the optimisation problem in the three-dimensional solution space into a set of optimisation subproblems defined on a two-dimensional solution plane and iteratively optimising all subproblems along two-dimensional coordinates, the solution gradually approaches the global optimum. Moreover, multiple objective functions are established in the context of SSA, and the decision-making process balancing these functions is embedded within each optimisation subproblem, leading the overall optimisation problem to converge towards enhanced performance in RSO catalogue maintenance.

The remainder of this paper is organised as follows: Section 2 introduces the mathematical principles of the Bernoulli Filter (BF) used for space object state estimation. Section 3 discusses the space-based observation model and the space object detectability model. Section 4 defines a general multi-sensor, multi-target tracking multi-step optimisation framework and further introduces the efficient high-dimensional multi-objective optimisation method developed. Section 5 presents detailed simulation results for large-scale tasking cases, where 12 space sensors track up to 1,000 LEO Starlink satellites over a 12-hour time window. Section 6 concludes the paper with discussion.

## 2. Bernoulli Filter

The developed optimisation method needs to be integrated with appropriate filtering techniques to obtain state estimations of space targets. The Random Finite Set (RFS) method captures the presence state of a target and its motion state in the surveillance region by modeling the state as a finite set of elements. The BF is a popular single-target tracker that developed based on the RFS theory. Compared with the classical Kalman filter, the BF measures the presence of a target using existence probability $r$, which accounts for the birth, survival or death of a target in the presence of detection uncertainty and environmental clutter, as well as missed detection. Because of these merits, the BF is a suitable tool in SSA as its effectiveness in detection and tracking.

Assume the orbital state of a space object is represented by a random variable $x$, and all the available information can be represented by a Bernoulli RFS $\pi = \{r, p\}$, where $r$ and $p$ represent the existence probability and probability density, respectively. If the posterior density $\pi_{k-1}$ at time $k-1$ is a Bernoulli given by $\pi_{k-1} = \{r_{k-1}, p_{k-1}\}$, with $p_{k-1}$ being a Gaussian mixture of the form

$$p_{k-1}(x) = \sum_{j=1}^{J_{k-1}} w_{k-1}^{(j)} \mathcal{N}\left(x; m_{k-1}^{(j)}, P_{k-1}^{(j)}\right) \tag{1}$$

where $w_{k-1}^{(j)}$, $m_{k-1}^{(j)}$ and $P_{k-1}^{(j)}$ are the weights, means and covariances of Gaussian component $j$, and $J_{k-1}$ is the number of Gaussian mixtures at time $k-1$. Then under linear Gaussian assumptions, the predicted Bernoulli RFS $\pi_{k|k-1} = \left\{r_{k|k-1}, p_{k|k-1}\right\}$ is given by

$$r_{k|k-1} = p_{R,k}\left(1 - r_{k-1}\right) + r_{k-1} p_{S,k} \tag{2}$$

$$\begin{aligned} p_{k|k-1}(x) = {} & \frac{p_{R,k}\left(1-r_{k-1}\right)}{r_{k|k-1}} \sum_{i=1}^{J_{R,k}} w_{R,k}^{(i)} \mathcal{N}\left(x; x_{R,k}^{(i)}, Q_{R,k}^{(i)}\right) \\ & + \frac{r_{k-1} p_{S,k}}{r_{k|k-1}} \sum_{i=1}^{J_{k-1}} w_{k-1}^{(i)} \mathcal{N}\left(x; m_{k|k-1}^{(i)}, P_{k|k-1}^{(i)}\right) \end{aligned} \tag{3}$$

where $p_{R,k}$ is the birth probability of targets, $p_{S,k}$ is the survival probability of targets, and $J_{R,k}$ is the number of the birth Gaussian mixtures at time $k$. $Q_{R,k}^{(i)}$ is the state covariances of birth-targets. And

$$m_{k|k-1}^{(i)} = F_{k-1} m_{k-1}^{(i)} \tag{4}$$

$$P_{k|k-1}^{(i)} = Q_{k-1} + F_{k-1} P_{k-1}^{(i)} F_{k-1}^{T} \tag{5}$$

Under linear Gaussian assumption, the prior Bernoulli UFS $\pi_{k|k-1} = \{r_{k|k-1}, p_{k|k-1}\}$ is updated using the collected measurement $Z_k$, and the posterior Bernoulli UFS $\pi_k = \{r_k, p_k\}$ is given by,

$$r_k = \frac{\left(1-p_{D,k}\right)\kappa_k^{Z_k} + p_{D,k}\sum_{z\in Z_k}\sum_{j=1}^{J_{k|k-1}} \kappa_k^{Z_k-\{z\}} w_{k|k-1}^{(j)} q_k^{(j)}(z)}{\frac{\left(1-r_{k|k-1}\right)}{r_{k|k-1}}\kappa_k^{Z_k} + \left(1-p_{D,k}\right)\kappa_k^{Z_k} + p_{D,k}\sum_{z\in Z_k}\sum_{j=1}^{J_{k|k-1}} \kappa_k^{Z_k-\{z\}} w_{k|k-1}^{(j)} q_k^{(j)}(z)} \tag{6}$$

$$p_k(x) = \frac{\left(1-p_{D,k}\right)\kappa_k^{Z_k} p_{k|k-1}(x) + p_{D,k}\sum_{z\in Z_k}\sum_{j=1}^{n|\kappa} \kappa_k^{Z_k-\{z\}} w_{k|k-1}^{(j)} q_k^{(j)}(z)\mathcal{N}\left(x; m_{k|k}^{(j)}(z), P_{k|k}^{(j)}\right)}{\left(1-p_{D,k}\right)\kappa_k^{Z_k} + p_{D,k}\sum_{z\in Z_k}\sum_{j=1}^{J_{k|k-1}} \kappa_k^{Z_k-\{z\}} w_{k|k-1}^{(j)} q_k^{(j)}(z)} \tag{7}$$

where $p_{D,k}$ is the detection probability of targets at time $k$, and $\kappa_k$ is the clutter intensity at time $k$. And

$$q_k^{(j)}(z) = \mathcal{N}\left(z; \eta_{k|k-1}^{(j)}, S_{k|k-1}^{(j)}\right) \tag{8}$$

$$\eta_{k|k-1}^{(j)} = H_k m_{k|k-1}^{(j)} \tag{9}$$

$$S_{k|k-1}^{(j)} = H_k P_{k|k-1}^{(j)} H_k^T + R_k \tag{10}$$

$$m_{k|k}^{(j)}(z) = m_{k|k-1}^{(j)} + K_k^{(j)}\left(z - \eta_{k|k-1}^{(j)}\right) \tag{11}$$

$$P_{k|k}^{(j)} = P_{k|k-1}^{(j)} - P_{k|k-1}^{(j)} H_k^T \left[S_{k|k-1}^{(j)}\right]^{-1} H_k P_{k|k-1}^{(j)} \tag{12}$$

$$K_k^{(j)} = P_{k|k-1}^{(j)} H_k^T \left[S_{k|k-1}^{(j)}\right]^{-1} \tag{13}$$

In practice, the detection probability $p_{D,k}$ is not time-invariant due to the variations in illumination conditions and relative distance between sensors and targets. The calculation of the correct $p_{D,k}$ plays an important role in the above process. For the multi-step sensor tasking problem, $p_{D,k}$ needs to be determined by the Apparent Magnitude (AM) and geometric position visibility of the target, which will be discussed further in Section 3.

## 3. Space-based Observation Model

Currently, SSA (Space Situational Awareness) missions are primarily conducted using ground-based sensors. However, with the increasing number of RSOs (Resident Space Objects), ground observation systems face challenges in terms of capacity, accuracy, and update frequency. On the other hand, the success of certain space-based SSA projects has demonstrated their ability to provide better coverage, higher accuracy, and faster revisit times [5,6]. Therefore, there is a growing need for further research into space-based multi-sensor task assignment methods for tracking large numbers of RSOs.

The state of the space-based sensor or target in LEO is usually expressed in terms of $\boldsymbol{r}$ and $\boldsymbol{v}$, which are defined in the J2000 Earth-Centered Inertial (ECI). When calculating the AM of a target, the topocentric spherical coordinate system is commonly used to determine the relative state between the sensor and the target.

When a dozen space-based sensors are confronted with thousands of potential observation targets, determining the detectability of targets using simple geometric relationships can significantly reduce the complexity of the solution space of the sensor control vector $\boldsymbol{u}$. The detectability of a target is jointly determined by its visibility, AM, and a constant target detection probability $P_D$ that measures the sensor profile, then $p_{D,k}$ can be expressed as

$$p_{D,k} = p_{v,k} p_{am,k} P_D \tag{14}$$

where $p_{am,k}$ is calculated according to the relative position among the target, the sensor and the Sun. The detailed derivation can be found in Coder [7]. The visibility $p_{v,k}$ can be further expressed as

$$p_{v,k} = (1-p_{b,k})(1-p_{s,k}) \tag{15}$$

where $p_{b,k}$ denotes the probability that the target is blocked by Earth, which is obtained from the geometric relationship among the sensor, the target and the Earth. The output of the function is 0 if the target is not blocked by the Earth in the FOR of the sensor, and it equals 1 if it is blocked. $p_{s,k}$ represents the probability that the target is blocked by the Earth shadow, which is obtained from the geometric relationship among the sun, the target and the earth. The output of the function is 0 when the target is not in the shadow formed by the sun to the earth, and it equals 1 when it is in the shadow. The geometric judgment methods for $p_{b,k}$ and $p_{s,k}$ are essentially similar, and the specific judgment method for $p_{s,k}$, for example, is shown below

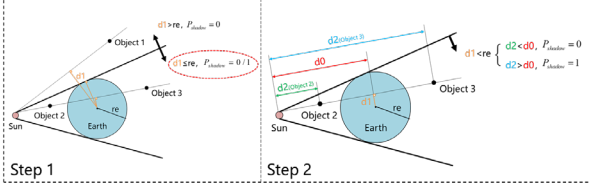

**Figure 1 The geometric judgment steps for $p_{s,k}$**

## 4. Sensor Tasking Optimisation

For the task planning of multiple sensors, single-step assignment strategies provide an effective approach due to their computational simplicity and quick response to anomalies. The core idea involves selecting the most valuable immediate observation task by maximizing a reward function or minimizing a penalty function, such as Information Gain (IG). The process of target state estimation and update driven by IG is illustrated in Figure 2. IG is calculated based on the predicted prior estimate covariance $P_{k|k-1}$ and the updated posterior estimate covariance $P_k$, with a larger IG value leading to more accurate posterior estimations [8]. Common IG functions include Kullback-Leibler divergence, Cauchy-Schwarz divergence, and Rényi divergence.

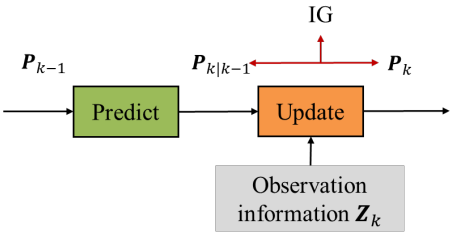


**Figure 2 Filtering process to compute IG using actual observation information**

Using the obtained IG, the single-step multi-sensor task assignment scheme can be modelled as a two-dimensional matrix, where each cell represents the IG value for each sensor-target pair. This matrix can then be optimised using auction algorithms [1]. However, the single-step assignment approach is inherently short-sighted, as it does not consider the overall effect over a time window during decision-making. Moreover, single-step methods often rely solely on mathematically defined reward functions without accounting for specific mission requirements, such as the apparent magnitude of space targets or the average observation intervals. Consequently, the use of a Predicted Ideal Measurement Set (PIMS) $\hat{Z}_k$ can replace actual observations $Z_k$, using $\hat{Z}_k$ to generate pseudo-posterior probability densities $\hat{P}_k$ and obtaining IG based on $P_{k|k-1}$ and $\hat{P}_k$., as shown in Figure 3. This extends the sensor tasking problem with $N_s$ sensors and $N_t$ targets from single step to multiple steps, which consisting $T_w$ epochs, considering the overall effect over time.

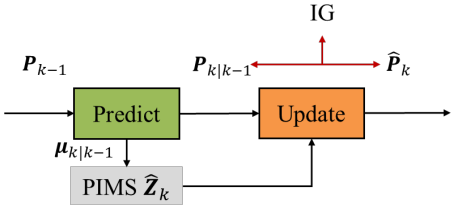


**Figure 3 Filtering process to compute IG using PIMS**

While multi-step task planning can consider the overall tracking effect over a time window, this also introduces challenges in optimizing the three-dimensional solution space. For example, when tracking hundreds of targets over thousands of time steps (epochs), the computational complexity becomes particularly significant. Therefore, a three-dimensional optimisation method must be developed that significantly reduces computational complexity while maintaining solution performance. Additionally, it is essential to incorporate mission-specific requirements to construct physically meaningful objective functions that guide the optimisation of multi-sensor task planning.

Thus, this paper models the multi-sensor multi-step task planning process as a three-dimensional optimisation problem, as shown in the left-hand side of Figure 4. The $x$-axis represents $N_p$ potential sensor pointing tasks, the $y$-axis represents $N_s$ sensors in the space-based tracking system, and the $z$-axis represents the time window $\{k, ..., k+T_w\}$, where $k$ is the initial epoch, and $T_w$ is the length of the time window, that is, each time window contains $T_w$ epochs. In this 3D solution space, element $(p,i,t)$ represents the task assignment $u_t^{(i,p)}$, where $u_t^{(i,p)}=1$ indicates that sensor $i$ is pointing $p$ at epoch $t$, and $u_t^{(i,p)}=0$ indicates it is not.

To reduce the dimensionality of the problem, sensor pointing number $p$ are used instead of binary 0-1 assignments, representing this three-dimensional optimisation problem in a two-dimensional task planning table, as shown on the right-hand side of Figure 4. The $y$-axis represents $N_s$ sensors, and the $z$-axis represents the time window $\{k, ..., k+T_w\}$. Each element $(i,t)$ in this two-dimensional solution space represents the task $u_t^{(i)}$, where element $u_t^{(i)}=p$ denotes the pointing number $p$ for sensor $i$ at epoch $t$.

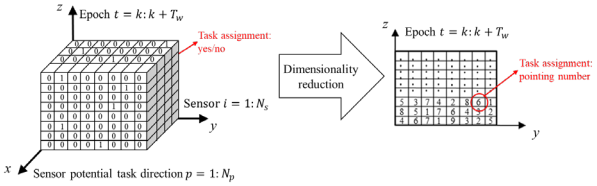


**Figure 4 Multi-sensor and multi-target tracking task planning model**

To describe the optimisation process over a time window, we define:

$$\boldsymbol{u}^{(i)} = \{u_k^{(i)}, u_{k+1}^{(i)}, ..., u_{k+T_w}^{(i)}\} \qquad (16)$$

representing a set of tasks for sensor $i$ over the time window $\{k, ..., k+T_w\}$. The tasks for all sensors over the time window are then defined as:

$$\boldsymbol{U} = \{\boldsymbol{u}^{(1)}, \boldsymbol{u}^{(2)}, ..., \boldsymbol{u}^{(N_s)}\} \qquad (17)$$

The optimal task

$$\boldsymbol{U}^* = \{\boldsymbol{u}^{(1)*}, \boldsymbol{u}^{(2)*}, ..., \boldsymbol{u}^{(N_s)*}\} \qquad (18)$$

is mathematically expressed as:

$$\boldsymbol{U}^* = \arg\min_{\boldsymbol{U}} \text{or} \max \left[ \boldsymbol{f}_{obj1}(\boldsymbol{U}), \boldsymbol{f}_{obj2}(\boldsymbol{U}), ..., \boldsymbol{f}_{objN_f}(\boldsymbol{U}) \right] \qquad (19)$$

where,

$$\boldsymbol{f}_{obj1}(\boldsymbol{U}), \boldsymbol{f}_{obj2}(\boldsymbol{U}), ..., \boldsymbol{f}_{obj\,N_f}(\boldsymbol{U}) \qquad (20)$$

are $N_f$ objective functions. The solution of the optimal task assignment $\boldsymbol{U}^*$ is a multi-objective optimisation process, in which we find $\boldsymbol{U}^*$ from all possible task assignments $\boldsymbol{U}$, to minimize or maximize each objective function. However, in most cases, multiple objective functions conflict with each other, making it difficult to achieve a global minimum or maximum for all functions simultaneously. Therefore, $\boldsymbol{U}^*$ must be balanced between the different objectives to optimise multiple criteria simultaneously.

If a sensor's field of view (FOV) is focused on a single space target, then the $x$-axis of the potential sensor pointing assignments is defined as $N_t$ targets, the $y$-axis as $N_s$ sensors, and the $z$-axis as the time window $\{k, ..., k+T_w\}$, as shown in Figure 5. First, there are $N_t$ targets can be selected to observe for sensor $i$ at epoch $t$. By calculating their PIMS based on the observation model, reserving the targets with the detection probability above a certain threshold $N_t^{(i,t)}$ for sensor $i$ at epoch $t$. Repeating this process for $N_s$ sensors and $T_w$ epochs, making the 3D solution space can be compressed into a reduced hyper-dimensional space.

Subsequently, a optimisation subproblem is defined to determine which target should be selected from $N_t^{(i,t)}$ potential targets for sensor $i$ at epoch $t$. Solving this optimisation subproblem provides the observation target for sensor $i$ at epoch $t$. Repeating this process across $N_s$ sensors and $T_w$ epochs results in a two-dimensional sensor tasking table, where each element $(i,t)$ records the task assignment $u_t^{(i)} = j$ observing target $j$ for sensor $i$ at epoch $t$. Completing a round of all optimisation subproblems with $N_s$ sensors and $T_w$ epochs is one iteration.

Since the task assignment of sensors affects the value of the objective function in each optimisation subproblem, after completing the task assignment for the final sensor at the last epoch, we return to the first sensor and first epoch, continuing the iterative optimisation process in the hyper-dimensional solution space. This iteration continues until either the required number of iterations $N_{iter}$ is completed, or system performance criteria are met.

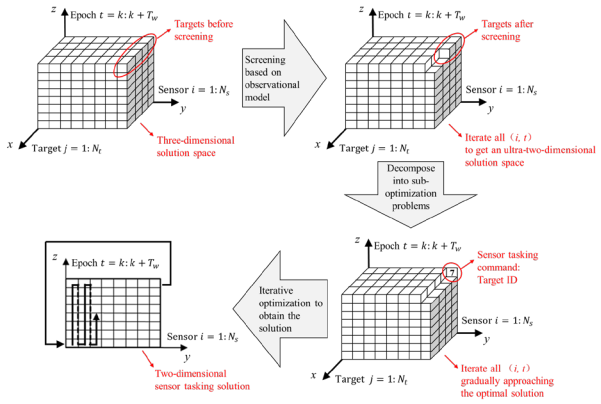


**Figure 5 Multi-sensor multi-step sensor tasking solution process**

The specific process of the optimisation method proposed in this paper is illustrated in Figure 6. Firstly, an initial task scheduling table is randomly generated from the high-dimensional solution space based on multi-sensor, multi-step task planning. The table is then optimised along the time epochs corresponding to each sensor. For each optimisation subproblem within the table's cell $(i,t)$, the values of $N_t^{(i,t)}$ sets of multiple objective functions are calculated when $N_t^{(i,t)}$ potential observation targets are respectively assigned to the sensor tasking solution. By balancing these objectives, the best target is selected from $N_t^{(i,t)}$ potential targets for the sensor $i$ at the epoch $t$. This process is repeated for all sensors and epochs, constituting one full iteration of the optimisation process. This iterative process is repeated until the objective functions fall below a certain threshold or the iteration count exceeds a pre-defined limit $N_{iter}$, yielding a task scheduling plan that meets the system requirements.

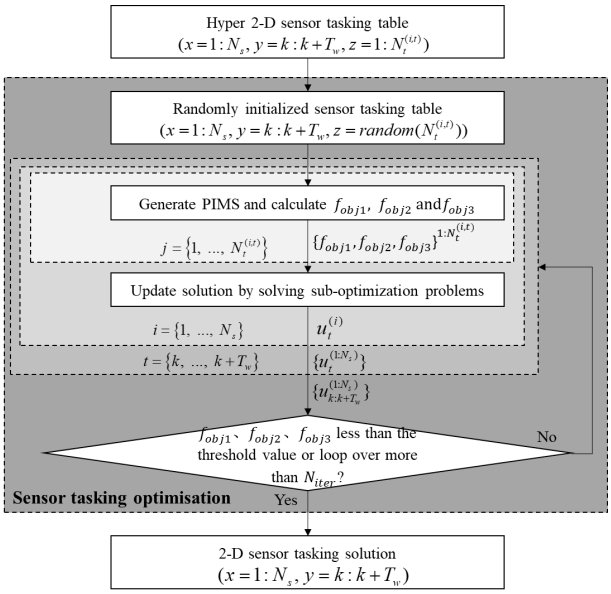


**Figure 6 Flowchart of traversal solution of optimisation subproblem**

The optimisation process guided by the objective functions can vary according to the task requirements in target tracking missions. These objectives may relate to detection quality, such as maximising detection probability, signal-to-noise ratio, or the number of successfully detected targets. Alternatively, they may concern cataloguing maintenance or orbit determination, such as the average number of detections per target or the time span between repeated detections. To improve the tracking performance of space-based observation systems for large-scale targets, three objective functions are designed in this paper to represent observation quality.

The first objective function is designed as the standard deviation of the number of detections for all targets, mathematically expressed as:

$$f_{obj1} = \sqrt{\frac{1}{N_t}\sum_{j=1}^{N_t}((N_d)^j - \overline{N}_d)^2} \qquad (21)$$

where $N_t$ is the number of targets, $(N_d)^j$ is the number of times target $j$ is observed within the time window, and $\overline{N}_d$ is the average number of observations for all targets during the time window. The smaller the value of this objective function, the more evenly the system can detect all targets.

The second objective function is designed as the average miss detection probability for all targets, mathematically expressed as:

$$f_{obj2} = \frac{1}{N_s T_w}\sum_{i=1}^{N_s}\sum_{t=k}^{k+T_w}(Q_d)_t^{(i)} \qquad (22)$$

where $(Q_d)_t^{(i)}$ is the probability that target $j$ is missed by sensor $i$ at epoch $t$, and this value matches $Q_d = 1 - P_d$ for any sensor at any epoch. The smaller the value of this objective function, the fewer the missed detections, indicating a higher total number of successful detections by the sensors.

The third objective function is the mean difference between the maximum and minimum intervals of adjacent detections for each target, mathematically expressed as:

$$f_{obj3} = \frac{1}{N_t}\sum_{j=1}^{N_t}(G_{max}^j - G_{min}^j) \qquad (23)$$

where $G_{max}^j$ and $G_{min}^j$ represent the maximum and minimum detection intervals for target $j$ within the time window. The smaller the value of this objective function, the more evenly the targets are detected over the time window.

For each optimisation subproblem, since the objective functions are interrelated and cannot be decomposed into independent optimisations for each, common strategies include minimising the sum or product of the objective functions. However, these strategies often fail to simultaneously minimise all objectives, potentially over-emphasising certain objectives at the expense of others. To address this, a Pareto front approach is employed in this paper to balance the conflicting objectives.

The core idea is to find the Pareto front in the three-dimensional space formed by the three objective functions, where the targets corresponding to solutions on the Pareto front can be considered equally optimal. A random solution from the Pareto front is selected as the solution to the optimisation subproblem, i.e., the observation target. As shown in Figure 7, the blue surface represents the Pareto front, and each point on the surface represents a solution. During the iterative process, solutions from the Pareto front gradually replace those falling off the front, enabling the optimisation process to explore the solution space more thoroughly and avoid local optima.

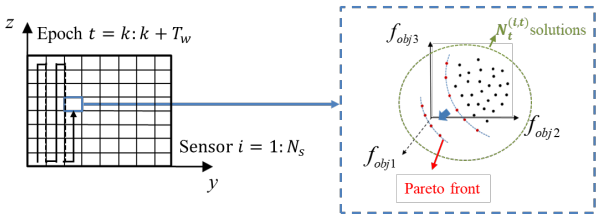


**Figure 7 Schematic diagram of solving optimisation subproblems based on Pareto frontier**

In terms of computational complexity, the proposed optimisation method offers a significant advantage over traditional exhaustive methods used to solve three-dimensional optimisation problems. The computational complexity of the exhaustive approach is $O(N^{(T_w \cdot N_s)})$, where $N$ represents the average number of observable targets per sensor at each epoch. As the number of epochs $T_w$ and targets $N_s$ increases, the computational burden grows exponentially, posing a severe challenge for large-scale target tracking optimisation. In contrast, the computational complexity of the proposed method is $O(N \cdot T_w \cdot N_s \cdot N_{iter})$, allowing the computational cost to grow linearly as the number of targets increases, significantly reducing the computational burden.

## 5. Simulation and Discussion

To evaluate the performance of the multi-sensor parallel tracking method designed in this chapter, a simulation was conducted using 12 space-based sensors to track 1,000 Starlink satellites. Each time window consists of 240 epochs, with a epoch interval $\Delta t$ of 1 minute, covering a total of 3 consecutive time windows, or 12 hours. The space-based observation constellation adopts a Walker constellation configuration, with parameters as shown in Table 1. It is assumed that each sensor in the constellation operates continuously and can reorient in any direction within a certain time $\Delta t$, constrained only by detectability.

**Table 1 Constellation parameters**

| Parameter | Value |
|---|---|
| Orbital altitude | 532.47 km |
| Orbital inclination | 46.86 deg |
| Right ascension of ascending node | 93.04 deg |
| Number of orbital planes | 4 |
| Number of satellites in the plane | 3 |

Since observational data and task decisions are obtained at discrete, uniform time intervals, it is assumed that targets can only be detected at specific epochs, and the detection epoch $t$ satisfies:

$$t = k\Delta t \qquad (24)$$

where $k = 1, 2, \ldots, T_w / \Delta t$. At these epochs, the state of the target is described by $X = [a, e, i, \Omega, \omega, M]$.

The true values of the initial states of each target are obtained from the publicly available catalogue information provided by NORAD on 15 January 2023, with the initial state uncertainties described by the covariance matrix in Table 2. The initial estimated states of the targets are generated by adding random perturbations due to uncertainties to the true values and converting them to Cartesian coordinates, which serve as the initial input for the filter. It is assumed that the orbital propagation of both satellites in the space-based observation constellation and the targets occurs in a two-body dynamics scenario.

**Table 2 Initial State Uncertainty**

| Parameter | Value |
|---|---|
| $\sigma_a$ | 10 km |
| $\sigma_e$ | $10^{-4}$ |
| $\sigma_i$ | $10^{-2}$ deg |
| $\sigma_\Omega$ | $10^{-2}$ deg |
| $\sigma_\omega$ | $10^{-2}$ deg |
| $\sigma_M$ | $10^{-2}$ deg |

During the observation process, each sensor generates an observation value $\boldsymbol{Z} = [\alpha, \delta]$ at each epoch, where $\alpha$ represents the right ascension and $\delta$ represents the declination of the target. The measurement noise and process noise for these observations are provided in Table 3.

**Table 3 Measurement Noise and Process Noise**

| Parameter | Value |
|---|---|
| Measurement noise (RA) | 5 arc sec |
| Measurement noise (Dec) | 5 arc sec |
| Process noise (position) | $10^{-4}$ km/s |
| Process noise (velocity) | $10^{-7}$ km/s |

The initial existence probability of a target is $r = 1$, its survival probability during state transition is $p_s = 0.99$, and the detection probability $p_{D,k}$ is calculated using the formulae given in Section 3, with the successful detection probability of the targets is $p_D = 0.98$. It is assumed that the clutter is uniformly distributed in the observation space according to a Poisson distribution with a mean of 1. The number of iterations for optimisation is set to $N_{iter} = 20$, and a total of 10 complete Monte Carlo (MC) simulations are conducted, with the average results of these 10 MC runs used as the basis for evaluation.

Upon completion of each optimisation subproblem during iterative optimisation, the values of the large-scale target tracking system on three objective functions are plotted in a coordinate system, demonstrating the convergence of each objective function during the optimisation process, as shown in Figure 8. For clarity of comparison, the values on the $x$-axis, $y$-axis, and $z$-axis are normalised between their maximum and minimum values. It can be observed that, after optimising the multi-sensor multi-step task scheduling, the three objective functions gradually converge from

larger values in the upper-right corner of the plot to smaller values in the lower-left corner. This indicates that the system achieves a more balanced detection of all targets, the total number of successful detections by the sensors increases, and the detection times for each target become more evenly distributed across the time window.

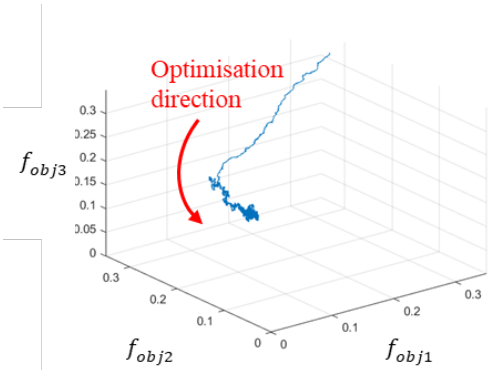


**Figure 8 Optimisation Process of the Three Objective Functions**

In the scenario where 12 sensors track 1,000 targets across 720 epochs, the proposed multi-step task scheduling method is compared with the IG-based single-step task scheduling method over 10 MC simulations in terms of sensor detection capability. As shown in Figure 9(a), the multi-step task scheduling method, based on multiple objective functions, improves the average detection probability of sensors from approximately 92% to about 99% compared to the single-step task scheduling method. This suggests that the multi-step task scheduling method is more predictive when selecting observation targets, thereby potentially collecting more observation results. Figure 9(b) further visually reflects this property, showing that the multi-step task scheduling method is more effective in utilising limited sensor resources.

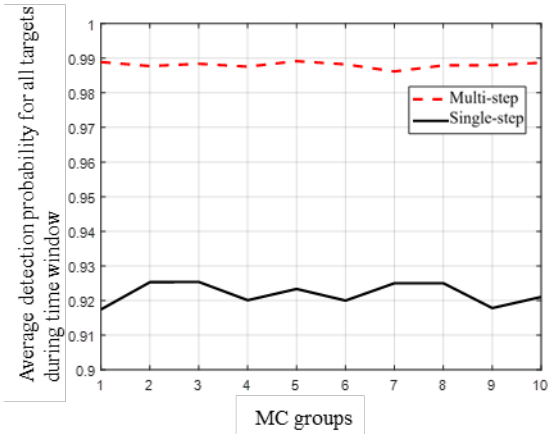


(a) Average Target Detection Probability

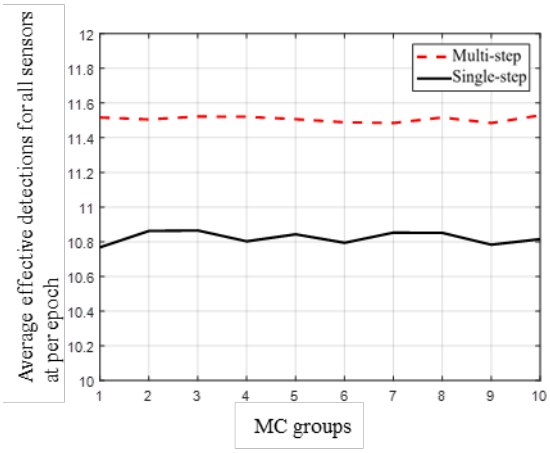


(b) Average Effective Detections per Time Step

**Figure 9 Comparison of Sensor Detection Capability between Multi-step and Single-step Task Scheduling Methods**

Further comparative analysis of the target tracking performance between the multi-step and single-step methods is conducted. The position error of the targets is calculated as the Euclidean distance between the estimated and true states, with the OSPA truncation parameter $c$ set to 100 km. The results of 10 MC simulations, where 12 sensors track 1,000 targets across 720 epochs, are plotted in Figure 10(a), and the average results of the 10 MC runs are shown in Figure 10(b). The results indicate that the multi-step task scheduling method reduces the peak value of the average position error by about 20% in the initial stage and by approximately 59% during the long-term tracking phase compared to the single-step task scheduling method, demonstrating the effectiveness of the proposed method.

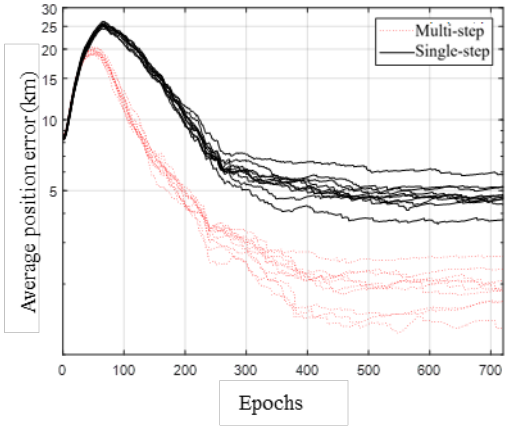


(a) 10 MC Results

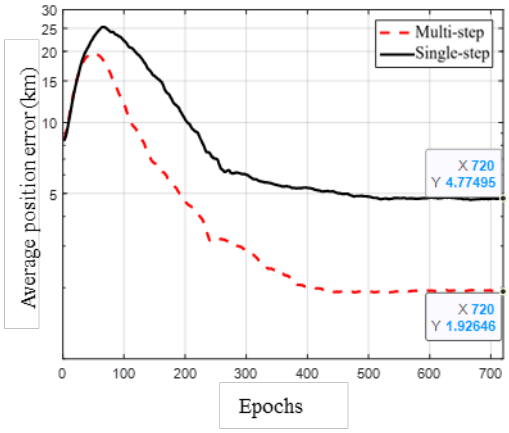


(b) Average Results of 10 MC Runs

**Figure 10 Comparison of Average Position Error between Multi-step and Single-step Task Scheduling Methods**

Similarly, the average velocity error in tracking large-scale targets using the multi-step method is compared with that of the single-step method, with the OSPA truncation parameter set to 0.1 km/s. The results of the proposed method after 10 MC simulations are shown in Figure 11. It can be seen that the trend of the average velocity error is similar to that of the average position error shown in Figure 10(b).

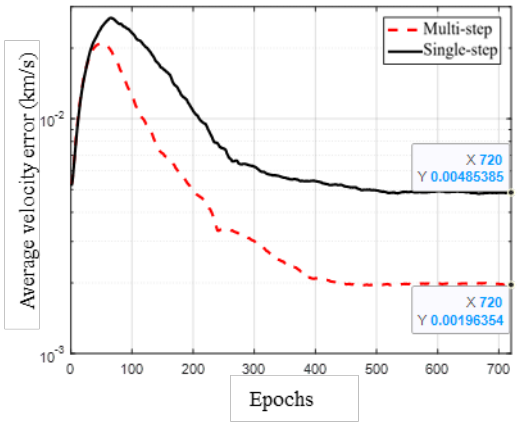


**Figure 11 Comparison of Average Velocity Error between Multi-step and Single-step Task Scheduling Methods (10 MC Average Results)**

In terms of maintaining the number of successfully tracked targets, the multi-step task scheduling method also demonstrates an advantage. Figure 12 records the variation in the number of successfully tracked targets over the time window, while Figure 13 presents the position errors of each target over the time window in the first MC simulation. Compared to the single-step task scheduling method, the multi-step task scheduling method can maintain continuous tracking of a larger number of targets. During the long-term tracking phase, the multi-step method is able to recover some of the targets that were lost in the early stages. This is attributed to the multiple objective functions established in accordance with the specific task context, which help maintain focus on each individual target. Specifically, while the IG-based single-step task scheduling method frequently abandons detection of certain targets due to lower IG values during allocation at each step, the multi-step task scheduling method, based on multiple objective functions, tends to detect all targets more evenly, thereby significantly improving the accuracy of tracking large-scale targets.

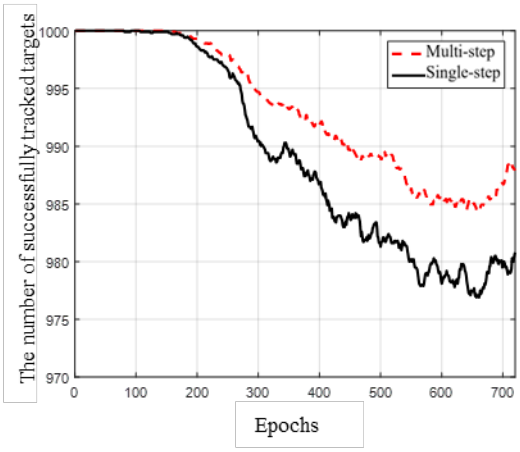


**Figure 12 Comparison of Successfully Tracked Target Numbers between Multi-step and Single-step Task Scheduling Methods**

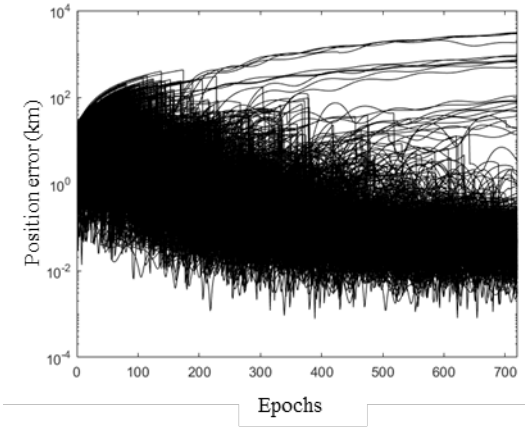


(a) Position Errors for Each Target in Multi-step Method

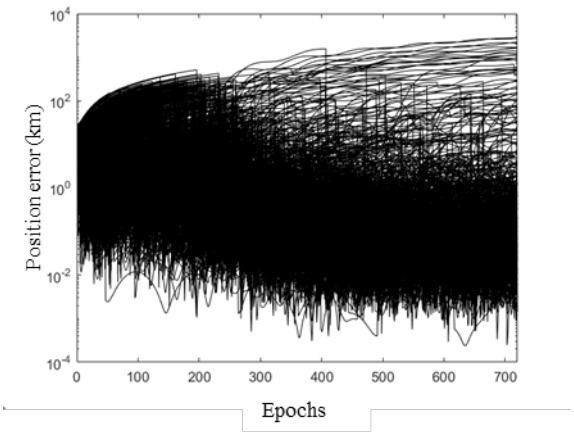


(b) Position Errors for Each Target in Single-step Method

**Figure 13 Comparison of Position Errors for Each Target between Multi-step and Single-step Task Scheduling Methods**

In terms of computational complexity, assuming 12 sensors observe 50 targets over 240 epochs with 20 iterations, the complexity of the exhaustive method is $50^{240\times12} \approx 10^{5760}$, while the complexity of the proposed optimisation method is $50\times12\times240\times20 \approx 10^{6}$, which demonstrates a clear advantage in efficiently tracking thousands of large-scale targets.

## 6. Conclusion and Future Work

This paper has presented an efficient optimisation method for large-scale sensor tasking in Space Situational Awareness (SSA) systems. By leveraging a multi-step optimisation framework based on coordinate descent and Pareto optimality, the proposed approach decomposes a complex three-dimensional solution space into manageable two-dimensional subproblems, progressively improving sensor tasking performance. The method effectively balances multiple conflicting objectives, such as detection probability, tracking accuracy, and catalogue maintenance, resulting in a substantial enhancement in tracking Resident Space Objects (RSOs) using limited sensor resources.

The multi-step optimisation method was validated through extensive simulations, where 12 space-based sensors tracked 1,000 Starlink satellites over a 12-hour period. The results demonstrate that the multi-step method outperforms the single-step Information Gain (IG)-based method by improving average detection probabilities, reducing position and velocity errors, and maintaining continuous tracking of a larger number of targets. The method's computational efficiency, achieved through dimensionality reduction and Pareto optimisation, further highlights its suitability for large-scale SSA applications.

While the proposed method offers significant improvements in sensor tasking efficiency, several avenues for future research remain. First, the integration of more sophisticated filtering techniques, such as those considering non-linear dynamics and measurement noise more accurately, could further enhance tracking performance. Additionally, incorporating real-time adaptability into the optimisation process could improve response times in dynamic space environments where RSOs' states evolve unpredictably. Finally, extending the current framework to address multi-sensor coordination across distributed networks, as well as exploring its applicability to new sensor modalities and emerging space surveillance technologies, will further contribute to SSA capabilities in an increasingly congested space environment.

## References

[1] S. Gehly, B. Jones, and P. Axelrad, "Sensor Tasking for Tracking Geosynchronous Space Objects," Journal of Guidance, Control, and Dynamics, Vol. 41, No. 1, pp. 149-163, 2018.

[2] K. M. Nastasi and J. Black, "An Autonomous Sensor Management Strategy for Monitoring a Dynamic Space Domain with Diverse Sensors," the 2018 AIAA Information Systems-AIAA Infotech @ Aerospace, Kissimmee, Florida, 2018.

[3] R. Linares and R. Furfaro, "An Autonomous Sensor Tasking Approach for Large Scale Space Object Cataloging," pp. 17, 2017.

[4] "Advances in Statistical Multisource-Multitarget Information Fusion" https://scholar.lanfanshu.cn/scholar?q=Advances+in+Statistical+Multisource-Multitarget+Information+Fusion.

[5] "SBSS (Space-Based Surveillance System) - Satellite Missions - eoPortal Directory." https://eoportal.org/web/eoportal/satellite-missions/content/-/article/sbss#foot12%29, (accessed 30.08.24)

[6] "Europe plans to launch space telescope to monitor orbital debris," 2021. https://www.space.com/orbiting-space-debris-telescope-esa.

[7] R. D. Coder and M. J. Holzinger, "Multi-objective design of optical systems for space situational awareness," Acta Astronautica, Vol. 128, pp. 669-684, 2016.

[8] Han C, Steve G, Yang Y. Reza Hoseinnezhad, Robert Norman, Kefei Zhang. Multisensor Tasking Using Analytical Rényi Divergence in Labeled Multi-Bernoulli Filtering[J]. Journal of Guidance, Control, and Dynamics,2019,42(9).